

**Supplementary Material: Theoretical Investigations of a Platinum-water Interface
Using Quantum Mechanics Molecular Mechanics Based Molecular Dynamics
Simulations**

R. P. Hardikar,^{1, a)} Unmesh Mondal,^{2, b)} Foram M. Thakkar,^{3, c)} Sudip Roy,^{3, d)} and
Prasenjit Ghosh^{4, e)}

¹⁾*Department of Physics, Indian Institute of Science Education and Research
(IISER), Pune 411008, Maharashtra , India*

²⁾*Department of Chemistry, Indian Institute of Science
Education and Research (IISER), Pune 411008, Maharashtra ,
India*

³⁾*Shell Technology Center, Bangalore, India*

⁴⁾*Department of Physics, Centre for Energy Science, Indian Institute of
Science Education and Research (IISER), Pune 411008, Maharashtra ,
India*

^{a)}Electronic mail: hardikar.rahul@gmail.com.

^{b)}Electronic mail: unmesh.mondal@students.iiserpune.ac.in

^{c)}Electronic mail: Foram.Thakkar@shell.com

^{d)}Currently at Akamara Therapeutics Inc. & Akamara Biomedicine Pvt. Ltd.

^{e)}Electronic mail: pghosh@iiserpune.ac.in

A. Validation of our modified SPC/E forcefield parameters for water: structural properties of bulk water at MM level

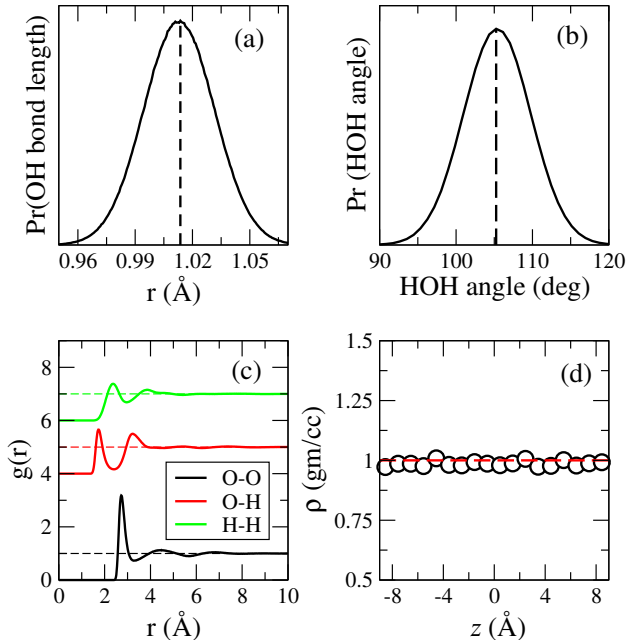


FIG. S1. Reproduction of structural features with the parameterized force constants K_b and K_θ for (a) OH bond distance and (b) HOH angle, respectively. Corresponding $g_{OO}(r)$ and plane average density distribution in z direction are shown in panels (c) and (d), respectively.

As mentioned in the main paper, we have modified the SPC/E forcefield. In our modified forcefield we use $K_b = 1600 \text{ kcal mol}^{-1} \text{ \AA}^{-2}$ and $K_\theta = 110 \text{ kcal mol}^{-1} \text{ rad}^{-2}$. With our new parameters we obtain an equilibrium bond length of 1.01 \AA for the OH bond and an equilibrium H-O-H angle of $\sim 105.5^\circ$ as shown in fig: S1(a) and (b), respectively. In an ideal SPC/E model the OH bond length is constrained to 1 \AA and H-O-H angle is fixed at 109.47° . The experimental value of H-O-H bond angle for bulk water is close to the average value of the angle that our forcefield parameters provide². Thus, our parameterized forcefields reproduce the intramolecular features correctly. Direct implication of the OH distance is the first solvation peaks in the $g(r)$. As shown in fig: S1(c), the first peak in $g_{OO}(r)$ is at a distance of 2.73 \AA . The experimental value of $g_{OO}(r)$ is 2.88 \AA^3 and corresponding value in case of SPC/E model is at 2.75 \AA^4 . Similarly, the first intermolecular peak in $g_{OH}(r)$ and $g_{HH}(r)$ are at 1.74 \AA and 2.36 \AA , respectively. In addition, the presence of second and third

solvation shell in $g_{OO}(r)$ matches well with literature and hence proves the validity of our forcefield parameter for water molecules.

B. Computation of layer resolved radial distribution function

The radial distribution function (RDF, $g(r)$) for a homogeneous fluid, which in our case is water, is given by:

$$g(r) = \left\langle \frac{n(r)}{v(r)} \frac{1}{\rho} \right\rangle, \tag{S1}$$

where $n(r)$ is the number of unique atom pairs at a distance of r and $r + \delta r$ (δr is the bin size of the histogram). As a consequence of periodic boundary condition(PBC), the maximum distance of r (r_{max}) is restricted to half of the shortest box length. $v(r)$ is the volume of the spherical shell at r of width δr and ρ is the particle density of the fluid. However, in our case, the system does not have a spherical symmetry because along the z direction we do not have periodic boundary conditions. There are two surfaces, one each at the Pt-water interface and at the water/vacuum interface. Hence special care needs to be taken for computing the RDF for the water molecules at the edges. Also, from our simulations, we find that at the Pt/water interface, the water molecules form distinct layers (at least two distinct layers can be identified as shown in Figure 2(b) of the manuscript). Hence, it would also be interesting to compute the RDF at different layers and compare them with bulk water. Here also we will encounter similar problems if one assumes spherical symmetry while computing the $g(r)$. Hence we need to compute the RDF taking special attention to the fact that spherical symmetry is lacking in our system.

To address these issues we have computed the RDFs for all the water molecules and the layer resolved ones with the method proposed by Kaya *et al.*⁵ Depending on the value of $r + \delta r$, the thickness of the water slab (h) and the distance of the reference atom (for which the $g(r)$ is being computed) from the edge of the slab (z), three distinct situations can arise as shown schematically in Figure S2: (i) the water molecule is completely surrounded by other molecules, thereby maintaining the spherical symmetry (Figure S2(a)), i.e. the spherical shell lies completely within the slab, (ii) the water molecule is close to the top or the bottom of the slab where part of the sphere (either from the top or bottom hemisphere) is cutoff because of absence of water molecules (Figure S2(b) and (c)) and (iii) part of the

sphere, from both the top and bottom hemisphere is cut off (Figure S2(d)). Hence for cases (ii) and (iii), we need correct for $v(r)$ by either removing the volume of the missing spherical caps from the volume of the spherical shell (for ii) or by considering volume of the spherical segment instead of that of a complete sphere (for (iii)).

The definition of volume for the different regions used in our calculations are given below:

1. Case (i) (Figure S2(a)): Here $(r + \delta r \leq z)$ and $(r + \delta r \leq h - z)$. The volume is given by:

$$v(r) = \frac{4}{3}\pi[(r + \delta r)^3 - r^3] \quad (\text{S2})$$

2. Case (ii) (Figure S2(b) and (c)): Here $(r + \delta r \leq z)$ and $(r + \delta r \geq h - z)$. To compute the volume, we need to subtract out the volume of the missing spherical cap from the volume of the sphere. If $p_1 (= (r + \delta r) - z)$ and $p_2 (= r - z)$ are the height of the spherical cap for spheres with radius $r + \delta r$ and r respectively, the the volume of the spherical caps are given by:

$$V_{scap1} = \frac{1}{3}\pi p_1^2[3(r + \delta r) - p_1]; \quad V_{scap2} = \frac{1}{3}\pi p_2^2(3r - p_2), \quad (\text{S3})$$

where V_{scap1} and V_{scap2} are the volume of the spherical caps corresponding to p_1 and p_2 . The volume $v(r)$ in this case is:

$$v(r) = V_{shell} - (V_{scap1} - V_{scap2}), \quad (\text{S4})$$

where $V_{shell} = \frac{4}{3}\pi[(r + \delta r)^3 - r^3]$ the volume of the spherical shell. In a similar way $v(r)$ can also be evaluated for Figure S2(c).

3. Case (iii) (Figure S2(d)): Here $(r + \delta r \geq z)$ and $(r + \delta r \geq h - z)$. For this case the shell is approximated by a cylindrical volume. $v(r)$ is given by:

$$v(r) = \pi h[(r + \delta r)^2 - r^2] \quad (\text{S5})$$

The number density (ρ) in Equation S1 is given by:

TABLE I. The thickness of the slab for the different layers and the full water slab.

System	h (Å)
Layer 1	2.5
Layer 2	4
Layer 3	5
Liquid layer	20

$$\rho = \frac{L_x L_y h}{N_{pairs}} \quad (\text{S6})$$

where, L_x and L_y are the box lengths along x and y axes, h is the thickness of each layer for the layer resolved $g(r)$ or the thickness of the complete water slab for the total $g(r)$. Pair selection, when $g(r)$ is to be computed for pairs having two different elements, for example $g_{O-H}(r)$ will be given by:

$$N_{pairs} = N_{setA} N_{setB} \quad (\text{S7})$$

where, N_{setA} and N_{setB} is the number of atoms of element A and B respectively. When the elements are same, for example for $g_{O-O}(r)$ and $g_{H-H}(r)$ the pair selection is given by:

$$N_{pairs} = 0.5 N_{setA} (N_{setA} - 1) \quad (\text{S8})$$

Incorporating all these, the $g(r)$ can be written as:

$$g(r) = \frac{L_x L_y h}{N_{pairs} N_{frames}} \sum_{k=1}^{frames} \sum_{i \in setA} \sum_{j \in setB} \frac{\delta(r - r_{ijk})}{v(r)}, \quad (\text{S9})$$

where, N_{frames} is the number of snapshots in the molecular dynamics simulation. Moreover, the δ function can be replaced by binning the pair distances(r_{ijk}) into a histogram of width δr as mentioned earlier. For this purpose, we have used a bin size of 0.2 Å. The different values of h used in our calculation is given in Table I.

C. Comparison between MM and QMMM simulations

Since we have performed MD simulations using both classical MD and QMMM MD, it is imperative to compare the results obtained from both the simulations. We note that while

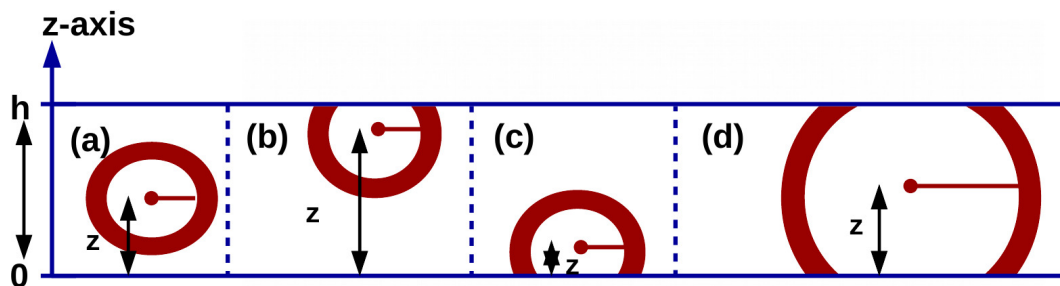


FIG. S2. Schematic for the four cases of spherical volume evaluation as a function of atomic coordinate in the direction of layer resolution. (a) The position of the reference atom is such that the whole sphere lies within the orthorhombic box. (b) The reference atom is towards the upper (lower in (c)) half of the box such that a spherical cap is cut off and (d) the reference atom is such that both the upper and the lower part of the sphere lies outside the box.

the MM simulations were performed for 9 ns, the QMMM simulations were performed for 10 ps. As a result the plots obtained from MM simulations are more smoother than those plotted with QMMM results.

While most of the properties, like layer resolved density (Figure S3), the $g(r)$ (Figure S4) and the population of zero, single and double H-bond donors at different layers (Figure S7), computed from the classical MD and QMMM MD are in qualitative agreement, the probability distribution (PDF) of the -OH bond length and the orientation of the water molecules at different layers obtained from the two simulations differ.

The -OH bond length PDF computed from QMMM MD trajectory (Figure S5(a)) shows that for the water layers near the Pt layers, there is slight shortening of the -OH bond length. In contrast, the layer resolved PDF obtained from the classical simulations (Figure S5(b)) shows same distribution for all the layers. The reason for this difference can be attributed to the choice of the classical potential chosen for our simulations. As described in Section 2.1 of the main manuscript and Section 1 of the Supporting Information, the force constants for the classical potential that is used to describe the O-H interactions in the MM region such that they mimic the results of the SPC/E water with constraints. Hence in the MM description of water, the -OH bonds are more rigid compared to that in the QM region.

The difference in the PDF of the orientation of the water molecules (Figure S6) is due to

the difference in the amount of statistics. While for the QMMM simulations we have used only 8 ps of trajectory, for the classical MD we have used about 9 ns of trajectory.

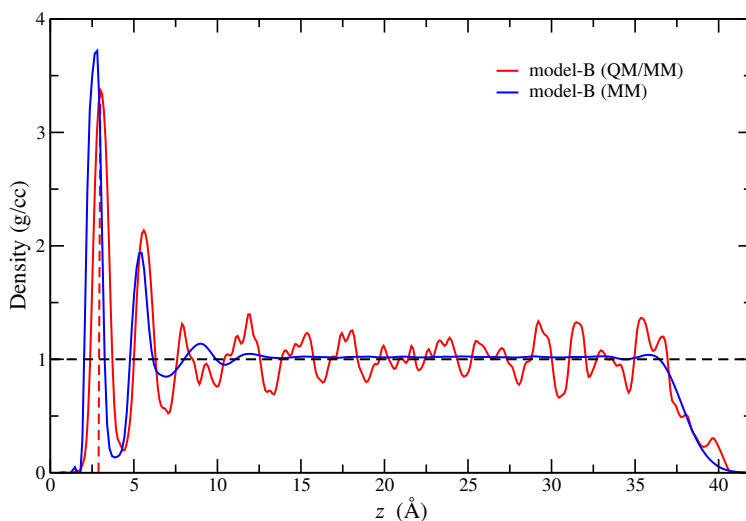


FIG. S3. Density of water in g/cc for water layers over the Pt surface for Model-B QMMM(red) and MM(blue).

REFERENCES

- ¹C. Vega and J. L. F. Abascal, “Simulating water with rigid non-polarizable models: a general perspective,” *Phys. Chem. Chem. Phys.* **13**, 19663–19688 (2011).
- ²J. Powles, “The structure of the water molecule in liquid water,” *Molecular Physics* **42**, 757–765 (1981), <https://doi.org/10.1080/00268978100100611>.
- ³A. Soper and M. Phillips, “A new determination of the structure of water at 25c,” *Chemical Physics* **107**, 47 – 60 (1986).
- ⁴P. Mark and L. Nilsson, “Structure and dynamics of the tip3p, spc, and spc/e water models at 298 k,” *The Journal of Physical Chemistry A* **105**, 9954–9960 (2001).
- ⁵S. Kaya, D. Schlesinger, S. Yamamoto, J. T. Newberg, H. Bluhm, H. Ogasawara, T. Kendelewicz, G. E. Brown Jr, L. G. Pettersson, and A. Nilsson, “Highly compressed two-dimensional form of water at ambient conditions,” *Scientific reports* **3**, 1074 (2013).

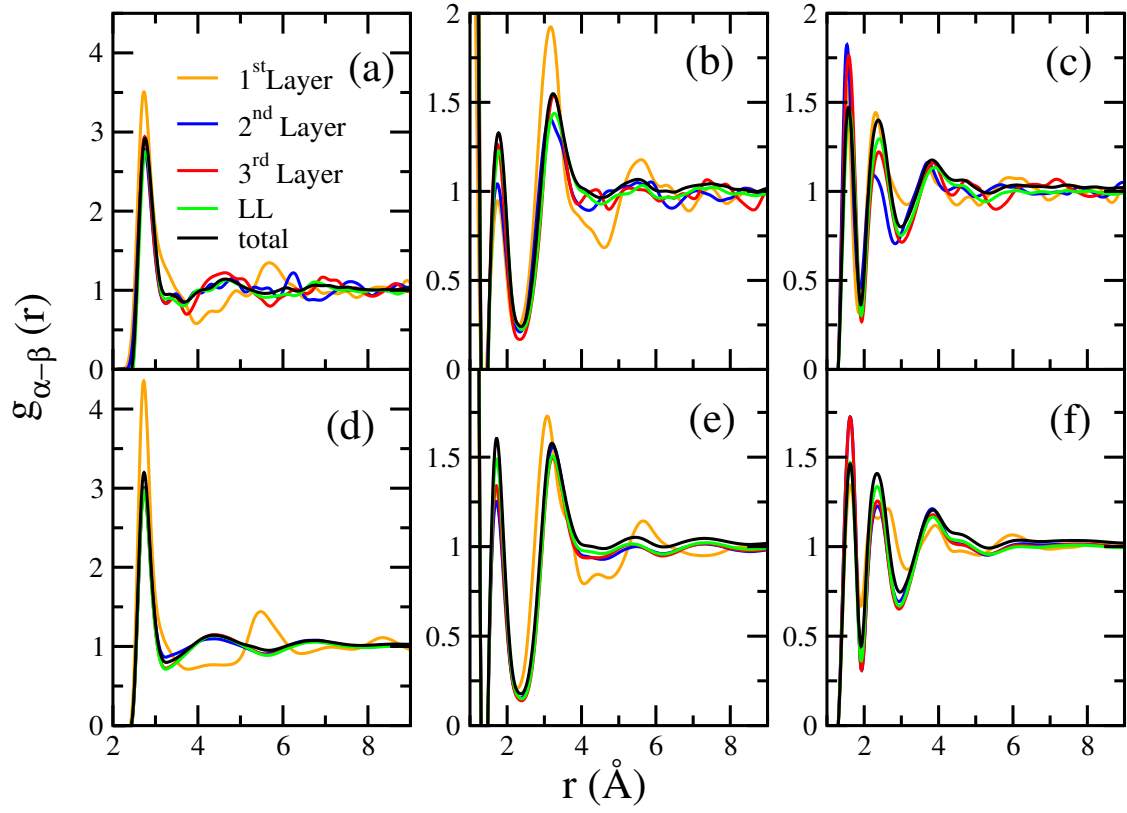


FIG. S4. (a)QMMM and (d) MM $g_{OO}(r)$. (b)QMMM and (e) MM $g_{OH}(r)$. (c)QMMM and (f) MM $g_{HH}(r)$.

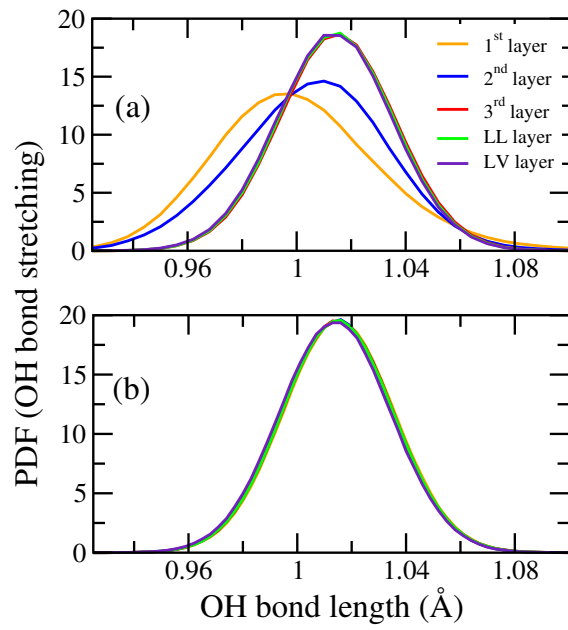


FIG. S5. Comparison of layer dependent probability distribution of -OH bond lengths between (a) QMMM and (b) MM.

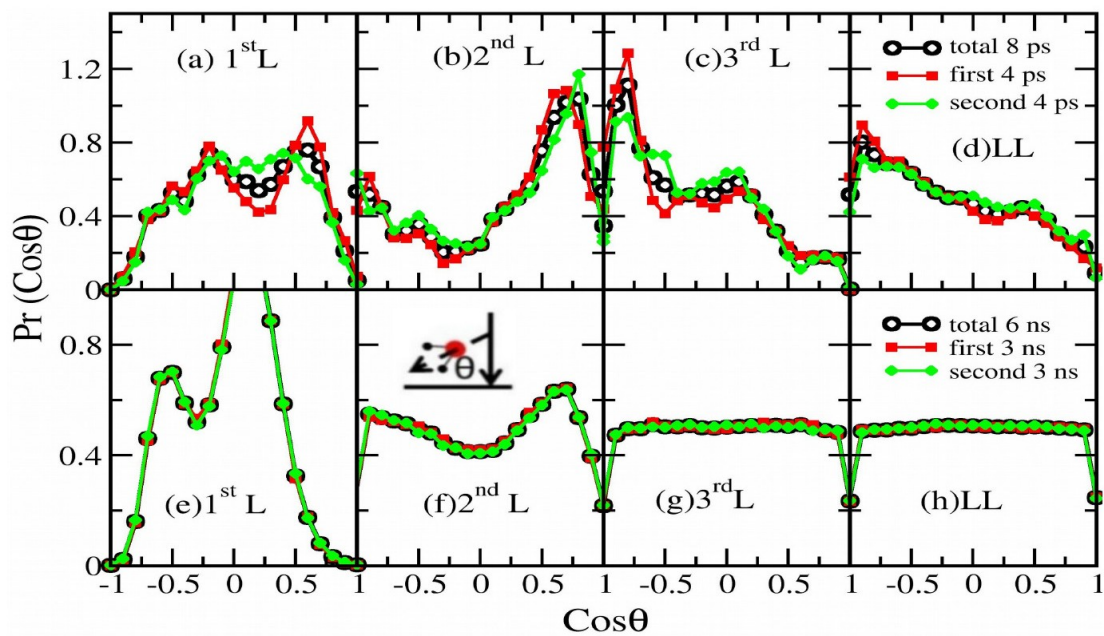


FIG. S6. Comparison of the probability distribution function of the angle between the geometric dipole vector of the water molecules in the water layer at the interface (1^{st} layer, a and e), those above it (2^{nd} layer, b and f, and 3^{rd} layer, g and c) and in the bulk liquid-like region (LL, h and d) with the surface normal for QMMM (top panel) and MM (bottom panel).

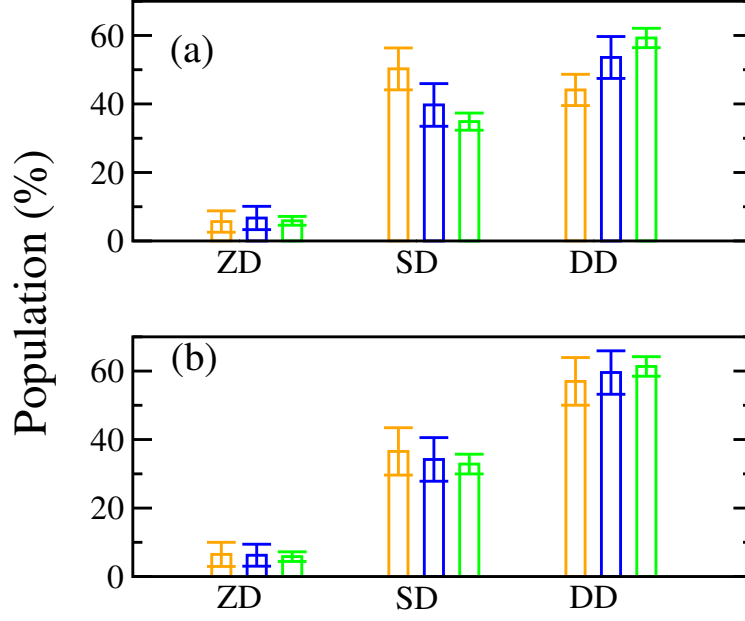


FIG. S7. Comparison between QMMM and MM results for layer resolved zero, single and double donors. For definition of the layers, the readers are referred to Fig. 2 in the main manuscript.

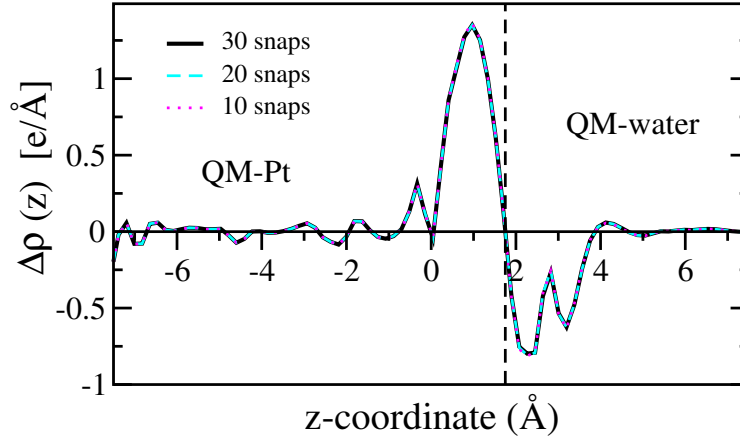


FIG. S8. Convergence of the charge transfer plot as a function of the number of snapshots used for computing the time average.